

Size estimation tools for conventional actuator system prototyping in aerospace

Gaétan Dussart* and Mudassir Lone†

*Cranfield University, Dynamic Simulation and Control Group
Cranfield, Bedfordshire, MK43 0AL, United Kingdom*

Ciaran O'Rourke‡

*Airbus Operations Ltd
Filton, Bristol, BS34 7PA, United Kingdom*

Predicting the size of an actuator capable of reaching given performance requirements is a critical step for any systems design. Thus, to help in the prototyping and early development stages of such devices, simple mathematical models were developed, which can be used with little knowledge in actuation system design. Based on physical phenomena at the heart of the actuation mechanism, these models can be used to estimate diameter and length, and therefore volume and weight of conventional actuators as a function of performance requirements. Models include linear hydraulic pistons and electric motors, divided into radial and axial flux machines. Off-the-shelf actuators and more aerospace specific products were used to validate and assess the accuracy of the models over a wide range of force and torque requirements. Simple sizing examples for aerospace actuation systems are also given as use-cases of the different tools. A discussion on model applicability, for various aircraft scales and applications concludes the paper.

I. Project Motivation

MULTIPLE actuator solutions are used in the aerospace industry today. In the civil aircraft design industry, system actuation solutions are almost exclusively dominated by hydraulic and electric systems. In fact, the actuation of landing gears and control surfaces has relied on hydraulic powered systems since the early days of assisted actuation, using centralised pumps and piping networks to distribute pressurised hydraulic fluid to pistons and rotary motors throughout the aircraft. In this centralised hydraulic philosophy, illustrated in Fig. 1a, hydraulic fluid is pressurised and distributed from a hydraulic accumulator, the Electric Driven Pump (EDP) and the system of interest (flap deployment system in this case). Recently, with the progress made in electric motor control and technology, the development of more electric aircraft control (MEAC) strategies have emerged. The main goal of this approach is arguably to reduce the weight, complexity, and redundancy to cope with failure rates dictated by hydraulic components[1]. Designers have had to rethink the aircraft internal systems layout, limiting hydraulic components where possible and optimising layout of the new systems. Centralised generators with global electric power distribution strategies are considered as potential evolutions with local Electro-Hydraulic-Actuators (EHA) or Electro-Mechanical-Actuators (EMA) where needed. A global layout sketch of the MEAC philosophy with an EHA system is given for flaps in Fig. 1b and with a EMA for ailerons in Fig. 1d. A flap actuation strategy relying on a mechanical shaft input is also given in Fig. 1c, for comparison.

Regardless of the system strategy being considered, space and weight allocation has always been a major concern for aircraft system design, especially in the restricted spaces near lifting surfaces. In both conventional and MEAC design philosophy, actuators will likely be placed as close as possible to the elements intended to be moved, ie. control surface or landing gear. For wing elements, this obviously forces designers to reduce the number and weight of mechanical linkage elements but also puts high constraints on the available space and sizing limitations. In some cases, such as flaps, additional fairings must be used to cover the elements linked with the motion of the high lift system.

These spatial and weight constraints have undeniably driven engineers and researchers to find new alternate solutions to conventional actuation, hinged joint and hard skins. Alternatives can be found in compliant structures, smart skins and shape memory alloys (SMA) [2–5], which are currently under the spotlight in various projects, as potential next

*PhD candidate, Dynamic Simulation and Control Group, g.x.dussart@cranfield.ac.uk

†Lecturer, Dynamic Simulation and Control Group, m.m.lone@cranfield.ac.uk

‡R&T Project Leader for Wing Architecture, ciaran.orourke@airbus.com

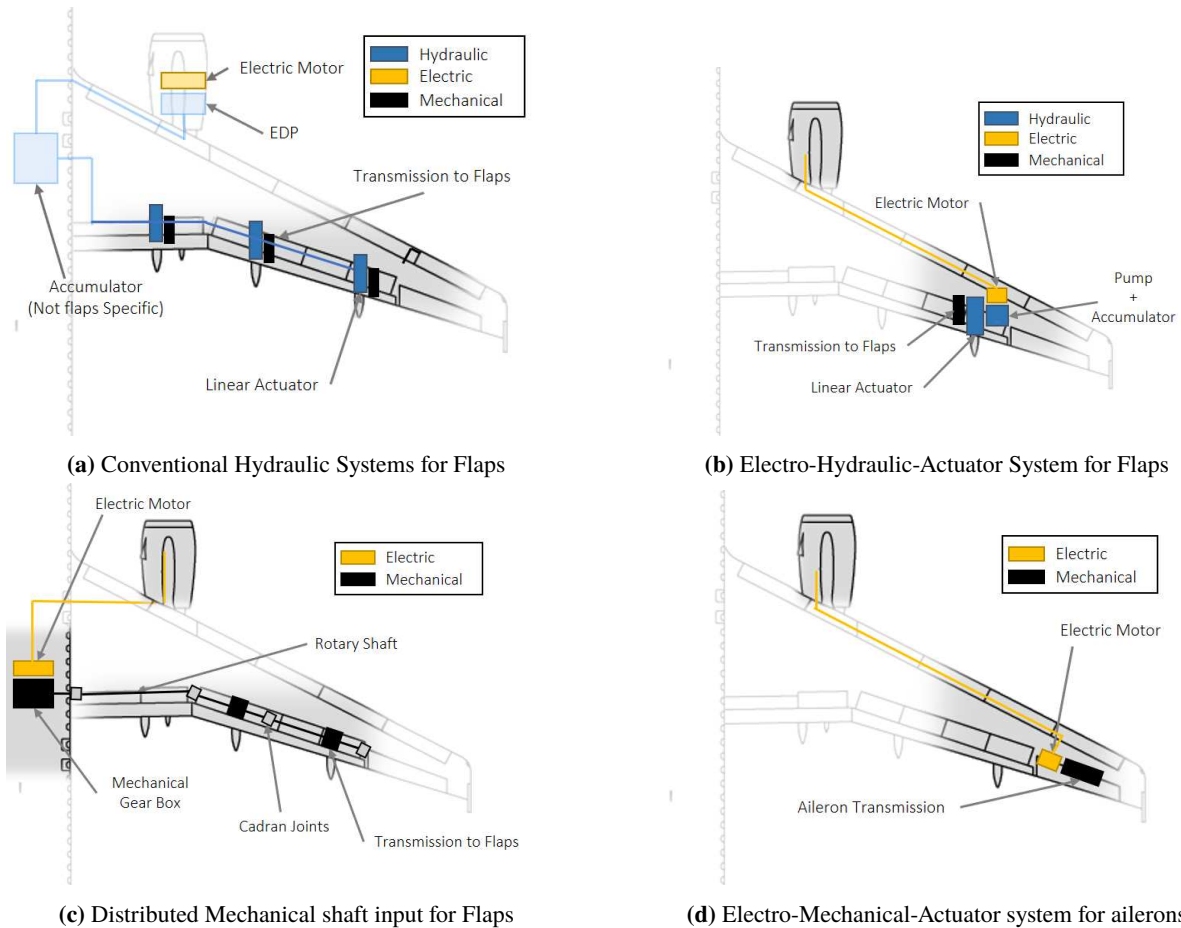


Fig. 1 Simple illustrations of the various system layout possibilities for flaps and ailerons actuated using linear hydraulic actuators or electric motors.

Note that the size of the actuator and various elements is not scaled relative to the aircraft. Furthermore, the path of the electric, hydraulic and mechanical links is not representative, but should serve as a general representation.

generation aircraft systems. But, with the exception of SMA, thermally or magnetically triggered, these new light weight solutions do not: 1. provide significant, if any, space benefits (compliant structures require complex structural webbing for instance, which does not increase system design space), and 2. most likely will still rely, at least partially, on conventional means of actuation, ie hydraulic and electric actuators. In other words, it is highly unlikely that hydraulic and electric actuators should disappear from aircraft in the near to moderate future, as significant work still remains before these devices can be used on large civil aircraft for instance.

Hence, the sizing of conventional actuator remains the common denominator in most actuation sizing problems in aerospace. Early estimations of actuator size during the design stage is paramount in order to evaluate the feasibility of the system, or assess how far a real actuator is from an ideal target for the system.

Specialised manufacturers likely use tools developed internally over the years, using old standard mathematical models updated to account for standards and preferences inherent to the company. Ultimately, data-sheets for the resulting off-the-shelf products can be found on websites or brochures. Some also provide basic sizing tools for potential customers to help identify the most suitable product given specific requirements. In any case, the customer is not required to understand the physics of the actuator, nor can he expect to always select the best available option with certainty. There is also an obvious lack of knowledge on sizing trends (diameter, length, weight...) as a function of requirement by using this approach.

Of course, off-the-bench actuator data can be used to generate sizing databases and get estimates of actuator sizing by data interpolation, or using scaling methods. Rapid sizing tools with appropriate levels of accuracy have been

developed in the past, specifically for EHA and EMA systems [1, 6–8]. Munjulury et al.[6] proposed their method to scale EHA and EMA used as control surface actuators based on physical mathematical models for hydraulic components and scaling laws for the electric actuator components. The outputs of their scaling method was then linked to a CAD software for space allocation within given design examples, in this case an aileron EHA. The framework Modalica has been used to scale electrical actuators [7, 8] based on comparison parameters (volume, mass), sizing parameters (required torque) and others, using geometric and power scaling laws relative to a reference off-the bench actuator. Electrical motors up to full aileron actuators can be designed using the framework, to relatively high level of details and complexity for a prototyping tool. This complexity comes with a cost in required user knowledge and set-up complexity, specifically in the electric motor details. The authors do mention that expert advice and help is provided in the tool, but set-up and use may still prove to be difficult for non advised users. Furthermore, the use of geometric scaling methods, based on single reference examples requires 1. a sufficiently large database to be available, and 2. small deviations relative to the selected reference model. It should also be noted that manufacturer preference and assembly style have a direct bias on the scaling approach. It is unclear whether design trends and potential beneficial parameters linked to machine size constraints can be easily identified using the previously introduced tools. The latter is a key feature for low actuator-knowledge engineers that may be looking into system sizing in spatially constrained environments.

Given these past developments, and on-going research activities in the scope of a wider actuator sizing project, the authors have identified the need for a simple physics based prototyping tools that engineers with low-level knowledge on actuators can use and understand, and which could be implemented in widespread software environments such as Matlab or even Excel. This paper introduces the mathematical models, simplifications and assumptions which were used and developed as a response to that need. Size estimates, and therefore volume and weight of commonly used electric and hydraulic actuators are obtained as a function of torque or force requirement based on physics based models for each actuation option, and not scaled relative to a database of reference actuator using a scaling approach. Alternatively, torque or force as a function of actuator size can be obtained. The sizing of these multi-purpose actuators, not constrained to specific control surface applications, was validated against empirical databases over an extended range of capabilities. In fact, these models are deemed suitable from large wind-tunnel or radio-controlled UAV models up to full scale civil aircraft actuators. However, these models are not intended to replace the thorough structural, thermal, magnetic or hydraulic flow analysis that will be required later on in the design stages, but help give quick and accurate estimate of various solutions that could be considered, without the need for complex simulation frameworks. The physics based model approach also highlights how spatial constraints of the design space can limit actuator capabilities, an advantage particularly useful in control surface or landing gear actuation, or more innovative wing morphing solutions. Overall, this paper aims to gather all the required data and methods to build conventional actuator sizing models for early system design stages. The hydraulic piston model is presented first in Section II. Both balanced and unbalanced options are considered in the model architecture, which led to a set of sizing data sheets. Similarly, the electric Radial Flux Motor (RFM) and Axial Flux Motor alternative geometry are then presented in Section III, along with their respective sizing data sheets as well. A couple of use case examples are then given in Section IV to illustrate the use of these models and potential applications, before moving on to a general discussion and conclusion regarding model applicability and potential further work in Section V.

II. Linear Hydraulic Pistons

In this section, a Linear Hydraulic Actuator Sizing (LHyAS) tool is presented in details, from the mathematical modelling assumptions made to the validation of the model against off-the-bench pistons, highlighting the wide applicability range of this model.

A. Motivation for Hydraulic Piston Actuator Sizing

Linear hydraulic actuators are widely used throughout an aircraft, relying on the hydraulic pumps and piping network available in the airframe. Traditionally, electric power harvested from the engine is used to power an hydraulic pump system, which then pressurises a pipe and hydraulic system network to the desired pressures. A schematic of the general layout of each component is given in Fig.1a, where the position of the pump in the engine, accumulator in the fuselage, and the actuators, dedicated to the flaps in this case, are clearly outlined. As outlined in the introduction, the MEAC design philosophy effectively translates into a switch from an hydraulic pipe network to an electric wire network. Where possible, hydraulic systems are replaced by their electric counterpart, or Electro-Hydraulic Actuators (EHA). These are compact systems that include an electric motor to drive and maintain an hydraulic actuation structure. Depending on the dimensions of the system, this EHA should be fitted as close to the system as possible.

In any case, hydraulic systems display high force densities for reasonably fast actuation rates, and are therefore unlikely to be replaced completely. Hence, if a piston is to be used, a size estimate must be made, as a function of actuation requirements, in order to design the system effectively at the early stages of development.

B. Linear Hydraulic Actuator Sizing Theoretical Model

Pistons, or hydraulic cylinders, are relatively simple actuation devices. A linear motion is achieved by exploiting the differential pressure forces acting on both sides of a slider, separating two adjacent chambers. Non-equilibrium in forces is obtained by changing the pressure in each of the piston chamber. Increasing pressure in one chamber whilst venting the other effectively leads to a sliding motion with a force F as function of the slider surface and pressure of the fluid or gas used. Pistons can be either balanced (designed to provide equivalent force in both directions) or unbalanced (with a stronger actuation direction). Fig.2 respectively shows basic diagrams of unbalanced and balanced hydraulic pistons, with the various important sizing variables used in LHyAS: actuator length L , stroke length L_s , rod diameter D_r , inner diameter D_i and outer diameter D .

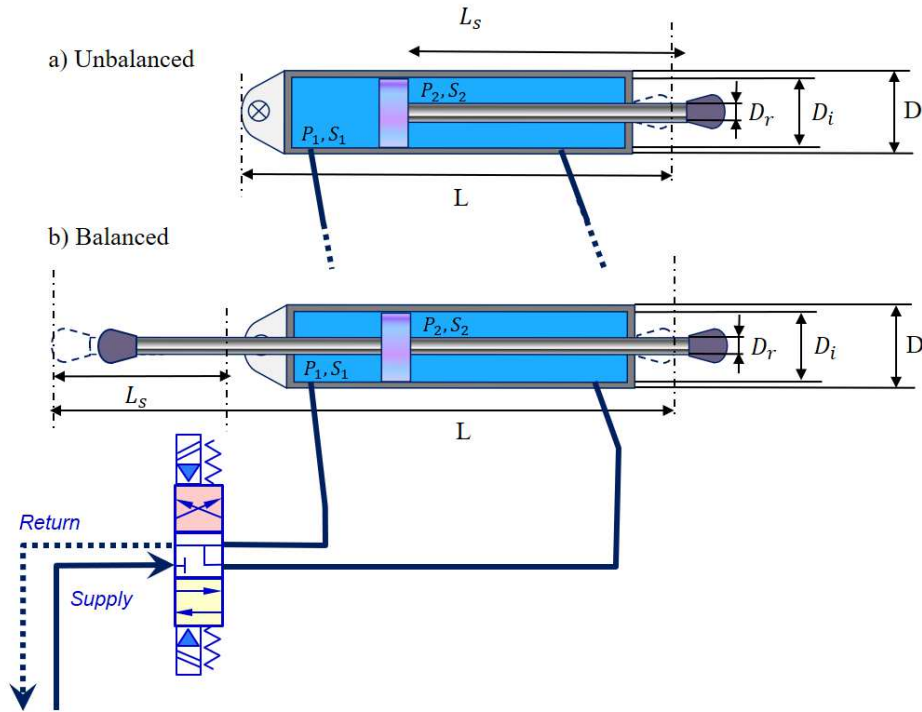


Fig. 2 Piston schematics for unbalanced and balanced actuators

The prediction of actuator rod diameter is a good starting point to start the sizing of the actuator, as the force requirement and stroke length will directly impact rod thickness. It is required to ensure that the central rod of the piston does not buckle under load. This can be done by calculating the rod section moment of area at the maximum stroke length using:

$$I_{rod}^{max} = \max(I_{rod}) = \frac{F \times (K_{buck} \times L_s)^2}{\pi^2 \times E} \quad (1)$$

where F is the required actuator force, K_{buck} is the buckling coefficient, L_s is the maximum stroke of the actuator, and E the elastic modulus (take $E = 200GPa$ for steel for example). The maximum rod section moment of area I_{rod}^{max} is then used to size the rod diameter D_r using Eqn.2.

$$D_r = \left(\frac{I_{rod}^{max} \times 64}{\pi} \right)^{\frac{1}{4}} \quad (2)$$

An illustrative example of changes in rod diameter with both force and stroke requirements is given in Fig.3 for a steel piston.

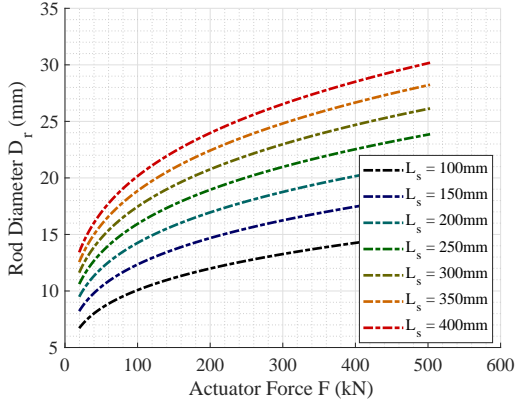


Fig. 3 Change in rod diameter D_r with force F and stroke length L_s requirements.

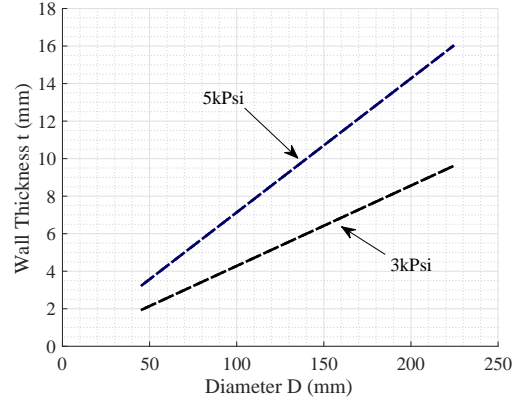


Fig. 4 Change in wall thickness t with diameter D and pressure P

Having established the relationship between force requirement, system pressure P and internal rod diameter D_r , we can now calculate the actuator inner diameter D_i following :

$$F = P_1 \times S_1 - P_2 \times S_2 \quad (3)$$

where P_1 and P_2 are the pressures in both piston chambers, and S_1 and S_2 are the effective cross sectional areas of the chamber separator. In a balanced actuator, $S_1 = S_2 = S$ where S is the area of the circle of diameter D_i minus the area of the circle of diameter D_r . Hence Eqn.3 becomes:

$$F = (P_1 - P_2) \times \left(\frac{\pi}{4} - (D_i^2 - D_r^2) \right) \quad (4)$$

where P_1 and P_2 are alternatively system pressure (3k Psi or 5k Psi for hydraulics of an aircraft for instance) and residual pressure, ideally 1 bar. Experimentally, we will see that this value is significantly higher. The next step is to calculate the thickness of the actuator to withstand system pressure.

The wall thickness calculations are based on the thin walled formulation using Hoop Stress. The thin walled cylinder pressure vessel σ_θ is given by:

$$\sigma_\theta = \frac{P \times \bar{D}}{t} \quad (5)$$

where P is the hydraulic pressure in Pascals, \bar{D} is the mean diameter of the cylindrical actuator, and t is the wall thickness. In order to establish t , the hoop stress must be set to the allowable stress σ_{allow} , which can be assumed to be:

$$\sigma_\theta = \sigma_{allow} = \frac{FTU}{2} \quad (6)$$

where FTU is the tensile ultimate stress of the material used (a value set at 483MPa for steel). Hence rearranging Eqn.5 and 6 for wall thickness t , we have:

$$t = \frac{2}{FTU} \times P \times \frac{\bar{D}}{2} \quad (7)$$

As a first step, the inner diameter D_i can be used to predict the wall thickness of an effectively smaller actuator. An iterative process using $D_i + t = \bar{D}$ leads to a convergence in t for the correct \bar{D}^* . Actuator outer diameter D is then simply found using:

* It is generally accepted that $D > 20 \times t$ should be respected when using thin wall theory. However, the authors believe that the target level of accuracy for this rapid prediction model allows for more relaxed conditions on t .

$$D = D_i + 2 \times t \quad (8)$$

Fig.4 illustrates the trend in wall thickness as a function of actuator outer diameter, for both 3k Psi and 5k Psi systems. The effect of hydraulic pressure and diameter is clear in Eqn.7 and Fig.4: if a 5k Psi system were to be used, a greater wall thickness would be necessary, ultimately increasing the outer diameter of the actuator. On the other hand, the reduced pressure of a 3k Psi would mean a greater diameter in the first place to reach the desired actuation force as the acting surface S would have to be greater.

With Eqn.1 to Eqn.8, an ideal theoretical model was generated. This model computes actuator outer diameter as a function of system pressure, stroke length and force requirement. It could also be used effectively as a means to compute the resulting force as a function of the actuator outer diameter.

This concludes the theoretical part of the LHyAS tool development, as actuator length L will strongly fluctuate with stroke length L_s , actuator type (balanced or unbalanced) and empirical data. Hence the next steps of model development have included empirical data for length prediction and model validation.

C. Empirical data for length estimation

An empirical database of balanced actuator length was fitted on a polynomial surface, in an attempt to extend the LHyAS model to include length L prediction. The surface fit is illustrated in Fig.5, where both the empirical data set (blue dots) and fitted surface are shown. The equation for the surface was found to follow:

$$L(x, y) = p_{00} + p_{10} \cdot F + p_{01} \cdot L_s \quad (9)$$

with coefficients p_{00} , p_{10} , p_{01} , given in Table 1. Using the polynomial equation, it is possible to carefully extend the actuator length calculations to actuation forces exceeding the limits of the database. A first order linear formulation was used instead of a second order polynomial term for actuator force F to ensure more realistic extrapolation results over slightly better interpolation match.

p_{00}	p_{10}	p_{01}	R^2	RMSE
60.66	0.8069	2.622	0.9999	6.384

Table 1 Polynomial term values and goodness of fit for $L(F, L_s)$

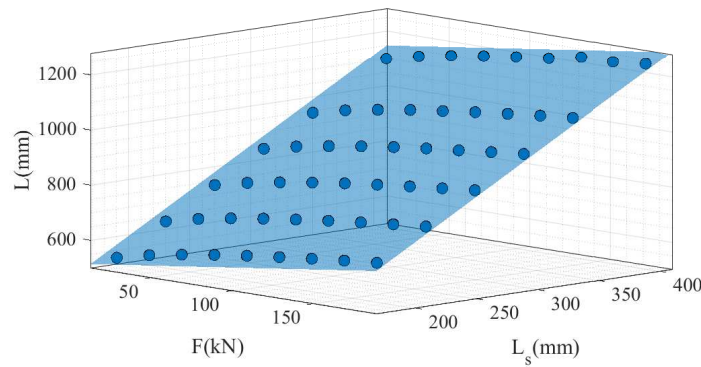


Fig. 5 Actuator length as a function of force and stroke from empirical data and a $L(F, L_s)$ polynomial surface fit.

As for the unbalanced actuator, the major difference that must be outlined is the lack of rod on one side of the slider, effectively making the unbalanced piston shorter by approximately a stroke length L_s . Hence, such a correction was used when sizing unbalanced actuators.

D. Validation of the hydraulic piston sizing tool

With a combination of both a theoretical approach to diameter predictions and empirical data for length estimations, it was key to compare and calibrate the piston theory against off-the-shelf products. In fact, most pistons are sized with safety factors in mind, and residual pressure in the non-pressurised chamber is never truly 1 bar. Therefore the model was modified to account for a user specified safety limit factor (set to $2/3$ in this dataset) to mimic the empirical database that was available during tool development. Hence Eqn.3 becomes :

$$F = \frac{2}{3} \times (P_1 \times S_1 - P_2 \times S_2) \quad (10)$$

Of course, this safety factor can be changed to any value depending on your acceptable limits. Similarly, a correction is applied to the rod diameter sizing.

Whilst comparing against an empirical database, covering actuation forces from $30kN$ to $130kN$, it was found that residual pressures of 20% or $P_2 = 0.2 \times P_1$ gave matching results. The now corrected and empirical models deviate by a maximum of 1% over the entire force spectrum using this correction.

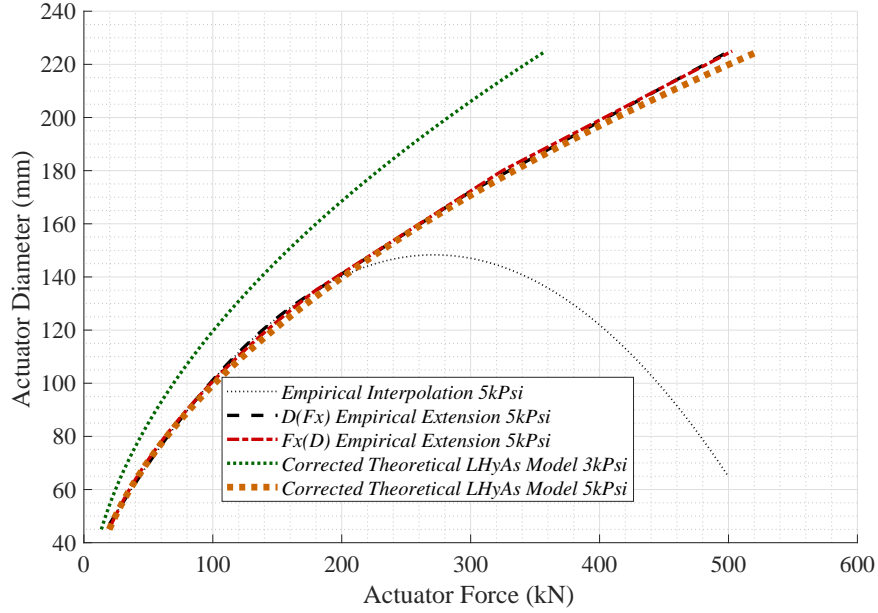


Fig. 6 Actuator Diameter as function of required force for various models.

Fig.6 highlights an interpolation model derived from the data of the empirical database, clearly unsuitable for predictions above $180kN$, as well as the corrected theoretical models for 3k Psi and 5kPsi. It also displays an upgrade to the previously used empirical interpolation model which predicted D as a function of F , $D(F)$, and vice versa $F(D)$, using piecewise linear extension to extend the empirical database. Overall, it can be seen that the corrected theoretical model built in the scope of this investigation gives the most satisfactory results.

To further validate the LHyAS tool, the unbalanced sizing option was used to predict the diameter and length of an actuator comparable to the one used for A350 landing gear deployment. Corresponding actuation force, including safety margin, required stroke and chamber pressures led to results off by just +2% in D and L , an accuracy level well above the authors original expectations when developing this rapid prototyping tool. Note that the latter actuator force requirements lie above the $500kN$, well over the limits of the original tool and database used to validate the lower end of the force requirement spectrum.

LHyAS, partially validated against empirical results, can now be used to size actuators of various actuation capabilities, such as control surfaces, deployable structures or landing gears. The mathematical model which was used was shown to be relatively simple and gives satisfactory results.

The sizing tool can be shortly summarised in the two following contour plots given in Fig.7 and Fig.8 . These charts are sized for 5k Psi, balanced steel pistons, with a safety factor of $2/3$ and residual pressure of 20%. Easy to

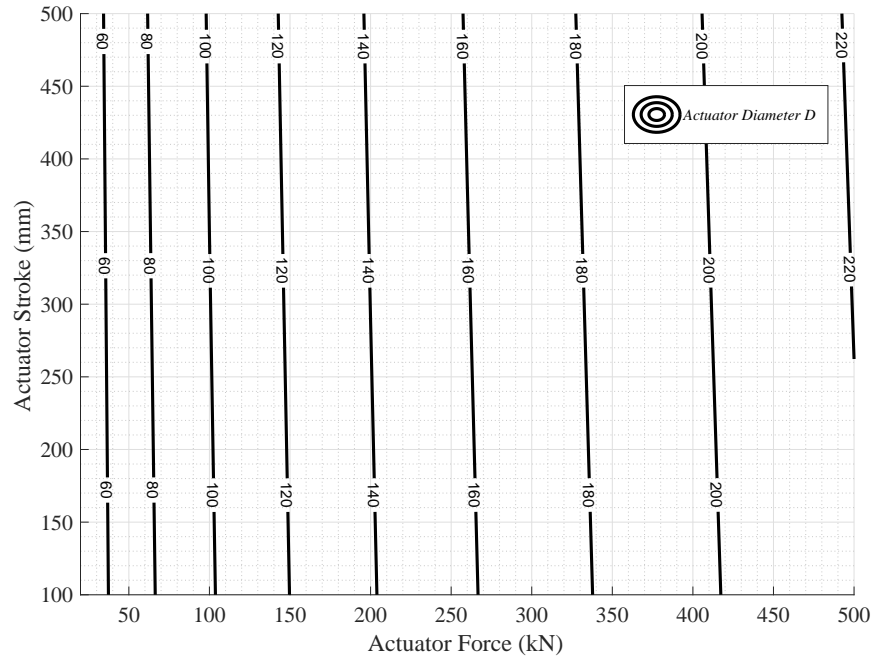


Fig. 7 D variations with force F and stroke length L_s

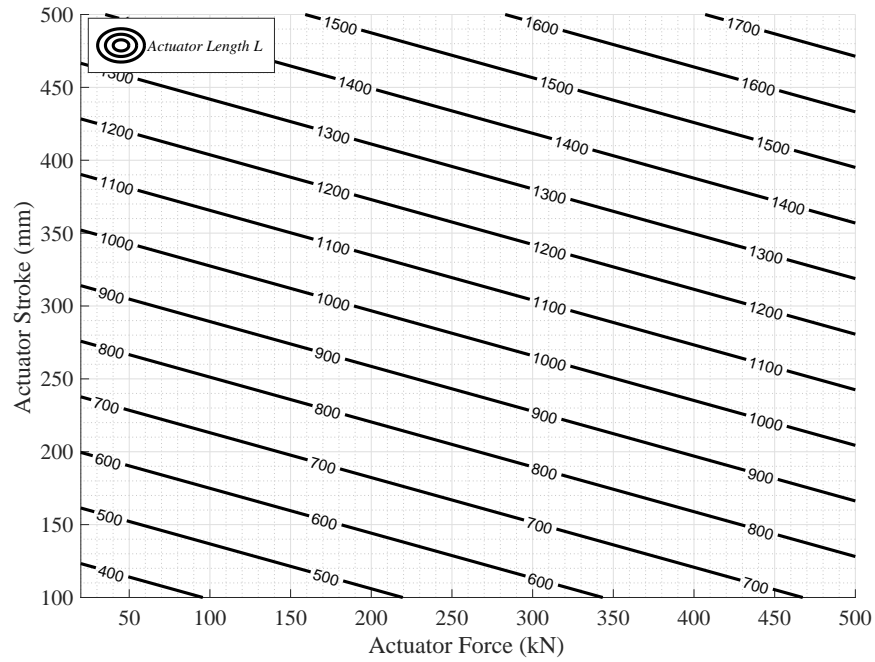


Fig. 8 L variations with force F and stroke length L_s

use, they can be used to quickly estimate the size of a piston, without the needs of any calculations. The first chart (Fig.7) highlights the impact of both required force F and stroke L_s on the actuator outer diameter D . The second chart (Fig.8) gives the value of actuator length L as a function of actuator force F and stroke L_s . Once a linear force, or moment and lever arm requirements are known, realistic actuator length and diameter can be determined instantly, with an overview on trends and achievable sizes. Using the above equation set, one should be able to construct similar sizing tools matching specific parameter requirements.

III. Electric Rotary Motors

In this section, a set of rotary electric motor sizing tool is presented. The modelling assumptions required to get an estimate of the radial and axial flux geometries are highlighted. Model validation was achieved against off-the-shelf products used in and outside the aerospace industry.

A. Motivation for Rotary Electric Motor Sizing

Electric motors are used to transfer electrical into mechanical power through the rotation of a shaft. These machines rely on the interaction between magnetic field and winding currents to generate forces or torque. For aerospace applications, electric motors are usually combined with gearbox to control output rotation speeds and torque. The motors can be used to pressurise hydraulic systems in an EHA for instance, or to drive a mechanical transmission shaft. The sketch in Fig.1d illustrates the conceptual layout of an EHA used to drive an aileron. Fig. 1c represents a mechanical drive shaft system for a set of flaps, with an electric motor and gearbox used to provide torque. Two types of electric motors, based on their geometry, are discussed herein: the Radial Flux Machines (RFM), and the Axial Flux Machines (AFM).

Radial Flux Motors have dominated the electric motor industry for nearly 150 years and display high rotation speeds with relatively high torques. They are comprised of a fixed stator and a rotating shaft called rotor, as sketched in Fig.9. In most cases, the rotor is housed within the stator in the shape of an hollowed out cylinder[†]. The latter is build as a stacking of thin laminated steel circular sheets. A triple phased coil powered by an alternative triple phase current runs up and down the stack inner diameter. When the phased current is applied to the wires, a rotating magnetic field is obtained. In an induction motor, the magnetic field induces a current in the cage structure of the rotor, which in turn generates a magnetic field and leads to a rotation of the rotor. For a permanent magnet machine, a natural magnetic field is already present which will naturally tend to align with any magnetic field generated by the electric current through the powered coils. A radial gap between the rotor outer diameter and stator inner diameter allows for the rotation of the rotor as both magnetic fields continuously align.

Similarly to the RFM, the Axial Flux Motor (AFM), sketched in Fig.10, is also comprised of a stator and a rotor. It differs in the geometry used, mainly with a change in flux orientation and position of both coils and permanent magnets (or induction wires) relative to each other. In this setup, the stator is a flat cylinder in which coils are arranged horizontally at the base within small slots. Permanent magnets or copper coils are arranged opposite of the stator within the similarly flat rotor disc. The penetrating magnetic flux is henceforth in the axial direction, hence the name of the machine[‡]. These motors tend to display higher torque densities and are significantly shorter than their radial counterparts. On the other hand, they are known to need greater diameters for a given torque requirement. They are also usually used with lower revolutions per minute (rpm). Nonetheless, AFM can be significantly boosted given a diameter limit, by using double stator configurations, as shown in Fig.10. This leads to significantly higher torque densities when compared to radial designs.

These type of motors have been more scarcely used than the radial counterpart, but the AFM has recently been put in the spotlights due to their recently highlighted potential applications[9–11]. Of particular interest is the prospect of using individual motors to provide torque to the wheels of an electric car or bike for instance. Their reversibility potential to be used as generators further complements this, and opens the possibilities for windmill applications as well. In fact, their potential for high positioning precision has also made them good candidates in medical equipment, a variety of vehicles and industrial equipment related to the oil industry.

Whilst in many way more complex than hydraulic pistons, it is still possible to predict the size of a machine based on the actuation requirements, though in no means do the authors claim that a thorough analysis later in the design phases becomes redundant.

[†] In some particular cases, such as small motors for radio-controlled vehicles, the outer housing can be used as the rotor whilst the inner core is used as a fixed stator

[‡] The flat layout of such machines have also earned them the nickname of 'pancake' motor.

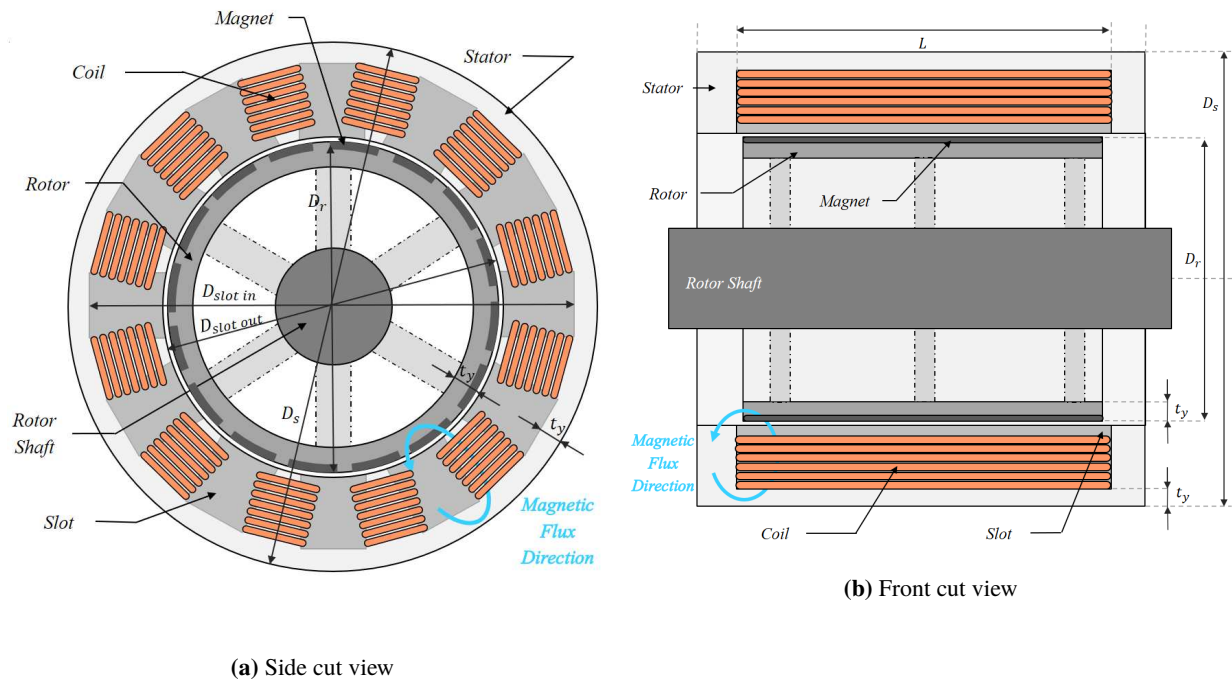


Fig. 9 RFM sizing sketches

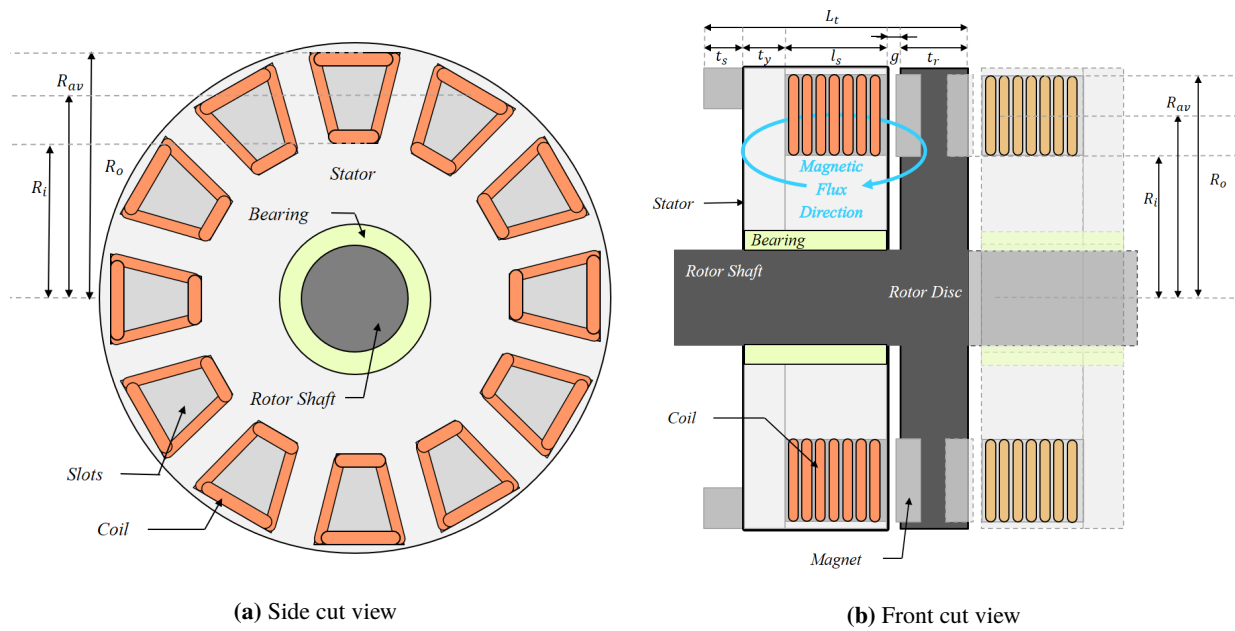


Fig. 10 AFM sizing sketches

B. Electric Radial Flux Motor Theoretical Model

To compute an estimate of the RFM, a mathematical model was derived in MATLAB: the Radial Flux Electric Motor Sizing (RFEMS) tool. It is based on a set of equations extracted from the literature [12, 13] which leads to an estimation of the RFM total diameter, length, rotor diameter, stack length and power as a function of many design variables. Whilst of great importance for later design stages, other characteristics such as current (nominal, stall, maximum), voltage, stator resistance and inductance, and efficiency are not considered at this stage. Note also that this approach neglects the losses in any way.

Firstly, in the case of an alternative current (AC) machine the synchronous speed n_s in revolutions per minute (rpm) is determined by the supply frequency f and the number of the machine pole pairs p such that :

$$n_s = \frac{60 \cdot f}{p} \quad (11)$$

The mechanical power required for a given mechanical torque T is then extracted using:

$$P = T \times n_s \times \frac{2\pi}{60} \quad (12)$$

where T and P are respectively the torque of interest and power requirements in $N.m$ and $Watts$. Assuming perfect efficiency (realistic values range from 0.85 to 0.95), this gives us a good estimate of the electrical power needed as well to run the machine. The rotor volume V_r of the machine can be expressed as a function of torque T and shear stress σ acting on the rotor (the product of electric and magnetic loading), following:

$$V_r = \frac{T_{req}}{2 \times \sigma} \quad (13)$$

with : $\sigma = B \times A$

where B is the uniform magnetic field and A is the linear current density. The shear stress σ has a typical value ranging from $20kPa$ to $35kPa$ in aerospace machines [13]. Rotor volume V_r can also be obtained by:

$$V_r = \frac{\pi}{4} \times D_r^2 \times L \quad (14)$$

where D_r is the rotor diameter and L is the rotor stack length. The reader is referred to Fig.9b and Fig.9a for annotated sketches of the RFM dimensions. Rotor diameter is generally set between 0.5 and 2 times the stack length. Hence, the dimensions of the rotor can be estimated for a given volume or torque requirement as a function of rotor diameter by making another assumption on the value of the stack length factor SLF such that:

$$L = SLF \times D_r \quad (15)$$

with : $SLF \in [0.5, 2]$

Therefore, external rotor diameter is given by:

$$D_r = \left(V_r \times \frac{4}{SLF \cdot \pi} \right)^{\left(\frac{1}{3}\right)} \quad (16)$$

With rotor volume and dimensions linked to torque requirements, the next step is to link the stator diameter and total length. In order to calculate the external stator diameter, another set of assumptions have to be made. Firstly, the stator slot ratio, or ratio between stator inner diameter at top and bottom of the coil slots, was fixed at $d = D_{slot\ out} / D_{slot\ in} = 0.7$ (See Fig.9a for illustration), a ratio demonstrated to lead to optimal torque results [13] for a given diameter. The ratio between the magnetic loading B (average air-gap magnetic flux density) and the peak yoke flux density B_y was also set to a conventional and acceptable value of $1/2.65$, which are intrinsically linked to the machine architecture. With these assumptions made, a value for the stator and rotor yoke thickness t_y can be derived using:

$$t_y = \frac{B}{B_y} \times \frac{\pi \cdot D_r}{4p} \quad (17)$$

With t_y obtained, it is now possible to calculate the stator external diameter D_s as it is proportional to the stator slot inner diameter and rotor diameter D_r plus twice the yoke thickness as given by Eqn.18. Note that the air-gap value was

neglected in the model. A small air gap is beneficial for magnetic efficiency but is detrimental to cooling and sustained machine performances.

$$D_s = \frac{D_r}{d} + 2.t_y \quad (18)$$

To finish, total or stator length L_s of the machine is obtained as a function of a D_r and stack length L given in Eqn.19.

$$L_s = L + l_f \times D_r \quad (19)$$

This empirical equation, crude and simple, is an attempt at capturing the real length of a machine that would incorporate casing and attachments on each side. It is undoubtedly the less reliable part of the model, with a length correction factor l_f set at 0.75 based on empirical data comparison. This was found to vary between manufacturers.

Hence, the model can now compute realistic dimensions in length and diameter for the radial flux machine as a function of torque. But having fixed quite a number of parameters through machine assumptions, it is of interest to investigate the impact of parameter variation on the overall sizing results.

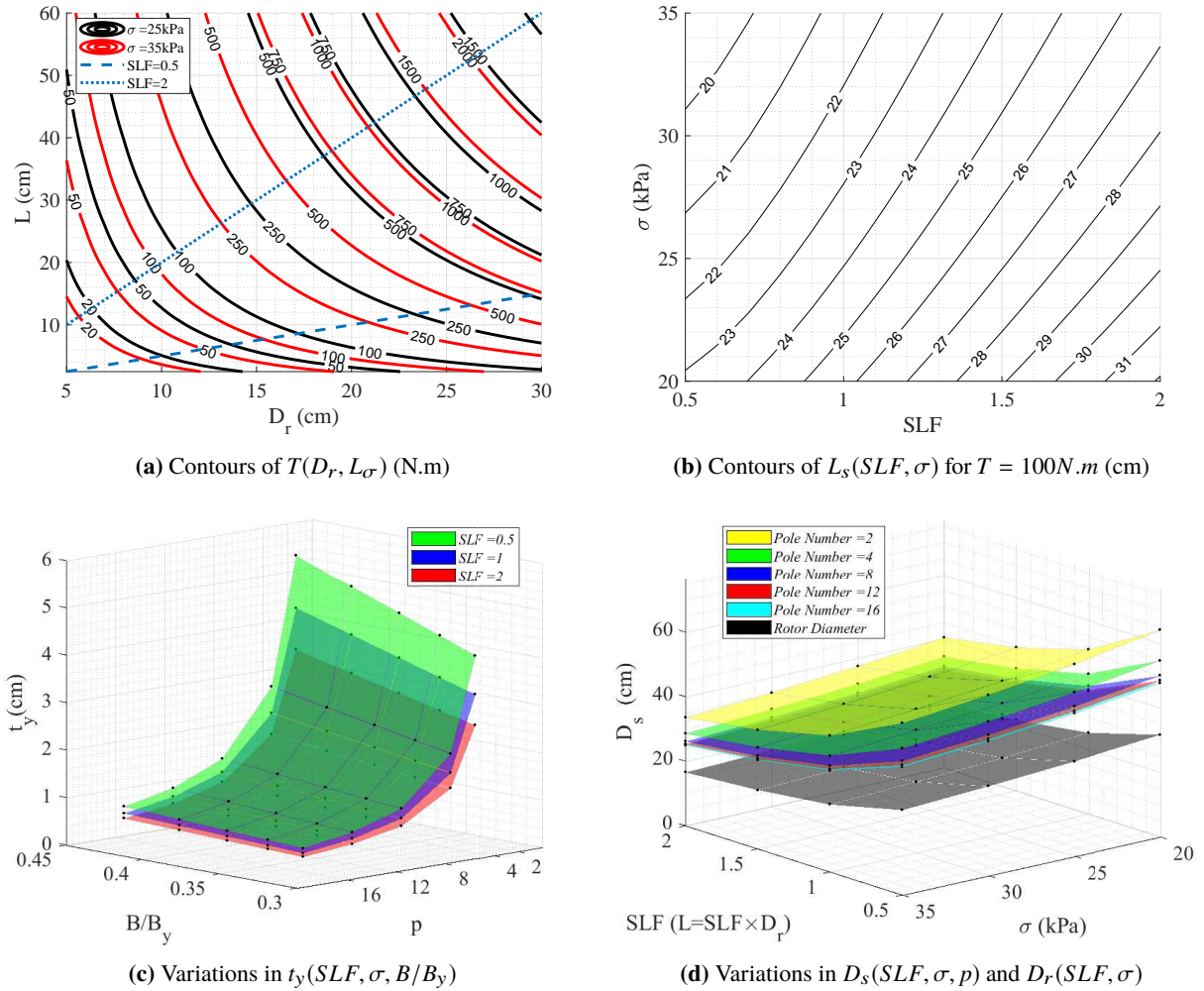
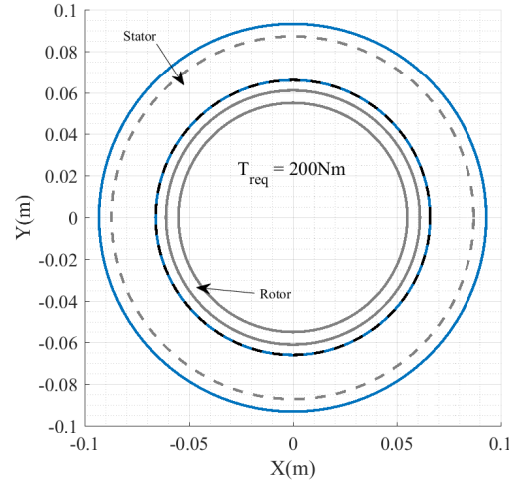


Fig. 11 Variations in RFM sizing variables following Eqn.14 to Eqn.19

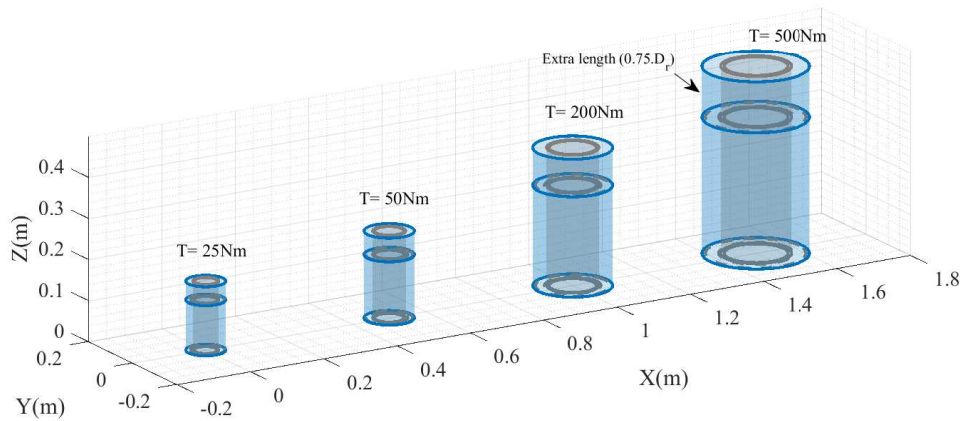
Fig. 11 illustrates the trends in sizing of the RFM with changes to key parameters of the machine. Firstly, Fig.11a illustrates the impact of changing both rotor diameter and stack length on the achievable torque, for two values of shear stress σ . It can be easily seen that for high torque in a reduced space, (small D_r and L), higher σ values are desirable, as expected. For a given torque T , increasing σ will also result in a reduction in rotor diameter D_r , and therefore overall

motor length, as shown in Fig.11b. The latter illustrates the change in motor length L_s with both σ and stack length L (or SLF). In that particular case, the torque was set to 100N.m which pre-constrained the value of D_r allowing for L_s to be computed following Eqn.19. Finally, the impact of changing the number of poles and B/B_y on the required yoke thickness is also highlighted in Fig.11c for a fixed torque requirement (again 100N.m) and three different values of stack length factors. From there it can be seen that increasing the number of poles drastically reduces the required yoke thickness, and that the impact of changing B/B_y reduces with p as well. This was found to be true for all SLF and torque values. Furthermore, it can be seen that increasing the stack length factor (and therefore reducing rotor diameter to follow the torque constrain) leads to smaller yoke thickness, reducing total stator diameter D_s following Eqn.18. This reduction in D_s with pole number $2p$ and stack length factor is also highlighted in Fig.11d as a function of σ where, once more, it can be seen that a higher σ should be prioritised in a spatially constrained studies. From Fig.11c and Fig.11d, we have also demonstrated that a higher number of pole would also greatly benefit the system, until a convergence is achieved at approximately 10 to 12 poles ($2p$).

Using D_s , D_r , L and L_s values, it is possible to verify the dimensions of the sized RFM, and appreciate the trends of T on the spatial volume of the motor, as shown in Fig.12b.



(a) Diameters for $T = 200\text{N.m}$



(b) Comparison of height and diameter of the RFM with T

Fig. 12 Sketches of different RFM sizing results

This particular sizing corresponds to a choice of $2p = 12$, $B/B_y = 1/2.65$, $\sigma = 35\text{kPa}$ and $d = 0.7$, $\text{SLF} = 2$

The sizing tool can once again be condensed to a set of contour plots. Quick estimates of rotor dimensions, without the needs for any calculations, can be made using Fig.13 to Fig.15. Firstly, a rotor diameter is obtained from Fig.13 for a given SLF and torque requirement. Total length can be obtained similarly in Fig. 14. Using the selected value for SLF, the adequate plot from Fig.15 is used to extract total diameter of the machine. Of course, instant and accurate results can also be achieved by running the script. Validation of the model is presented in Section III.D

C. Electric Axial Flux Motor Theoretical Model

Despite being similar in principle to RFM machines, the general layout and change in coil and magnetic flux orientation leads to AFM dimensions quite different to those of an equivalent torque/power RFM. Hence, a different mathematical model was built in MATLAB. The Axial Flux Electric Motor Sizing (AFEMS) tool was also based on a set of simplified equations extracted from the literature [14, 15] and analogies to equations used for the RFM sizing were used to estimate dimensions of an AFM. The AFM rotor outer diameter, stator width and total width can be computed based on a number of design variables. Once more, other characteristics such as current (nominal, stall, maximum), voltage, stator resistance and inductance, and efficiency will not be considered for this early sizing model. Note also that this approach neglects the losses in any way.

Similarly to the RFM, AFM synchronous speed and power can be computed using Eqn.11 and Eqn.12. Henceforth, the sizing approach differs, with the AFM sizing tool using the air-gap area A_{agap} , or magnetically active area opposing both stator and rotor. The reader is referred to Fig.10 for a visual representation of all design variables. Eqn.20 gives the value of A_{agap} as a function of the rotor active material outer diameter R_o and inner diameter R_i .

$$A_{agap} = \pi \cdot (R_o^2 - R_i^2) \quad (20)$$

A ratio between R_i and R_o , can be introduced as α_{ar} , purely to simplify problem formulation and respect common practice in the field of AFM design [14, 15]. Eqn.20 henceforth becomes:

$$A_{agap} = \pi \cdot R_o^2 (1 - \alpha_{ar}) \quad (21)$$

An average radius R_{av} is introduced in Eqn.22 and used to compute the rated torque that this machine can develop following Eqn.23 where σ , once again, stands for the magnetic flux shear stress.

$$R_{av} = \left(\frac{1 + \alpha_{ar}}{2} \right) \times R_o \quad (22)$$

$$T = \sigma \times A_{agap} \times R_{av} \quad (23)$$

Alternatively, the torque T can be expressed as a function of R_o and α_{ar} following a simple expansion, leading to Eqn.24

$$T = \sigma \times \pi \cdot R_o^3 \left(1 + \alpha_{ar} - \alpha_{ar}^2 - \alpha_{ar}^3 \right) \quad (24)$$

We now have a direct and simple relation between the torque and required outer diameter of the rotor of our AFM. Empirical evidence points toward a value of $\alpha_{ar} = 0.6$ as the best compromise between performance and cost [14]. Higher α_{ar} value leads to less magnetically active material (*greater* R_i) and therefore less force or torque applied. Meanwhile, a lower α_{ar} (or *lower* R_i) does not significantly boost torque despite an increase in magnetic material, weight and cost of the machine, as additional surface is placed near the shaft. This is illustrated in Fig.16b, where the torque T is plotted as a function of both α_{ar} and R_o . As an axial machine, R_o will dictate the radial size of the AFM, with a small margin for housing in the opposing stator.

Next, we need to size the axial length of the machine L_t , which will be the sum of smaller components following:

$$L_t = t_s + t_y + l_s + g + t_r \quad (25)$$

where t_y is the yoke thickness, l_s is the slot depth, or height of the coil stack, g is the width of the air-gap between stator and rotor, t_r is the rotor width, and t_s is the length of an eventual support, which could arguably be fitted on the sides of the stator, and therefore also stands as an additional sizing safety margin. In the case of a permanent magnet machine, the additional thickness due to magnet protuberance out of the rotor in the axial direction is not modelled in this formulation, and is transparent in the gap g term.

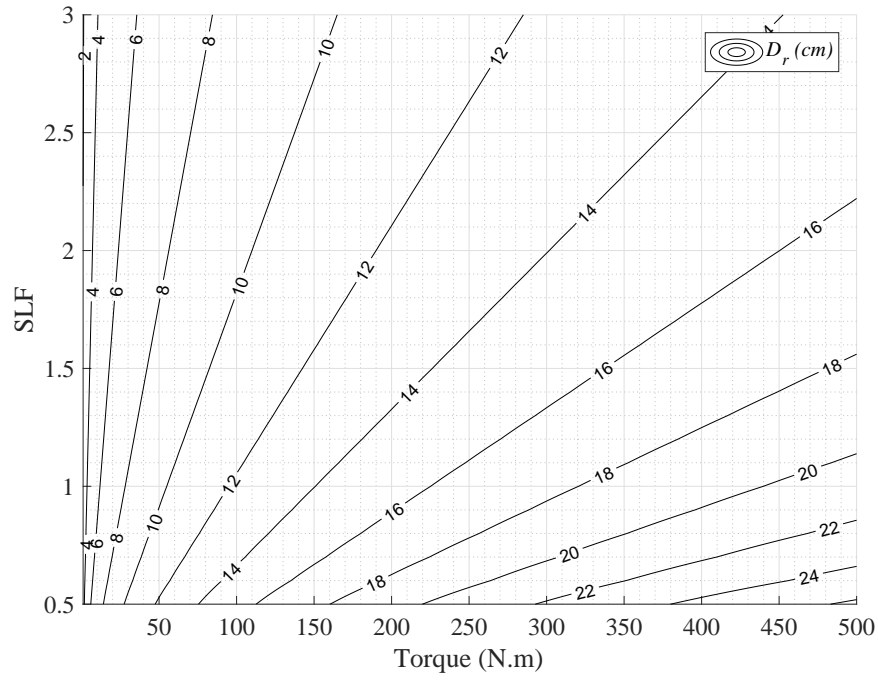


Fig. 13 D_r (cm) variations with torque T and SLF factor for $\sigma = 35 \text{ kPa}$.

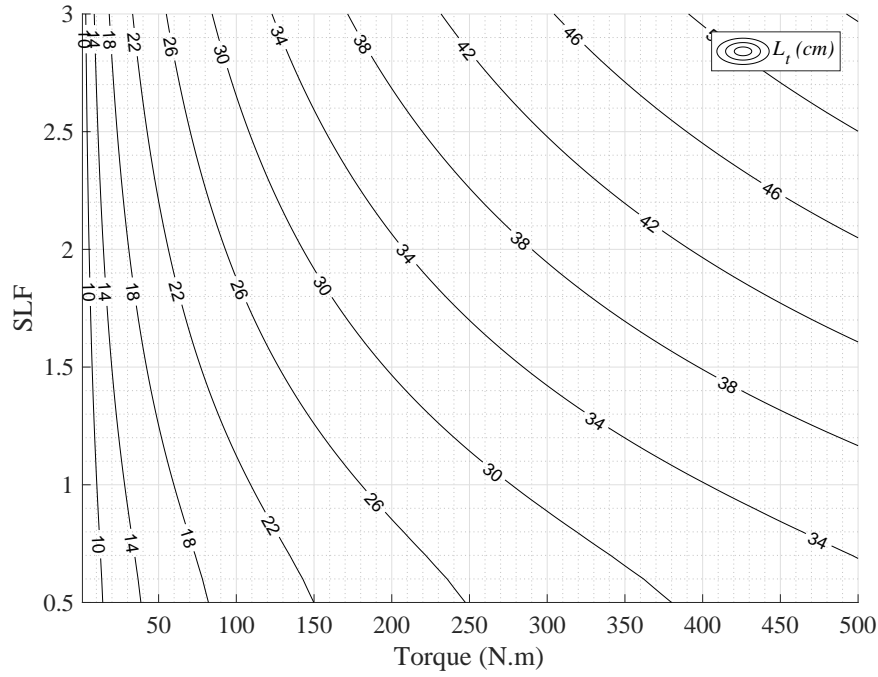
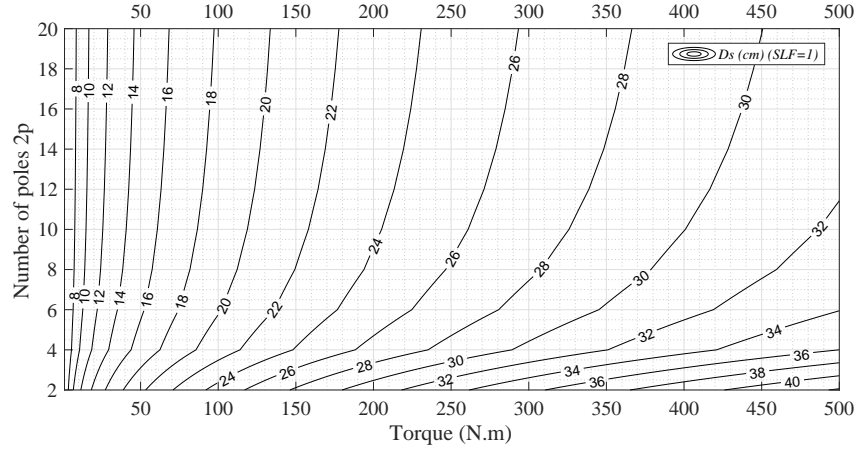
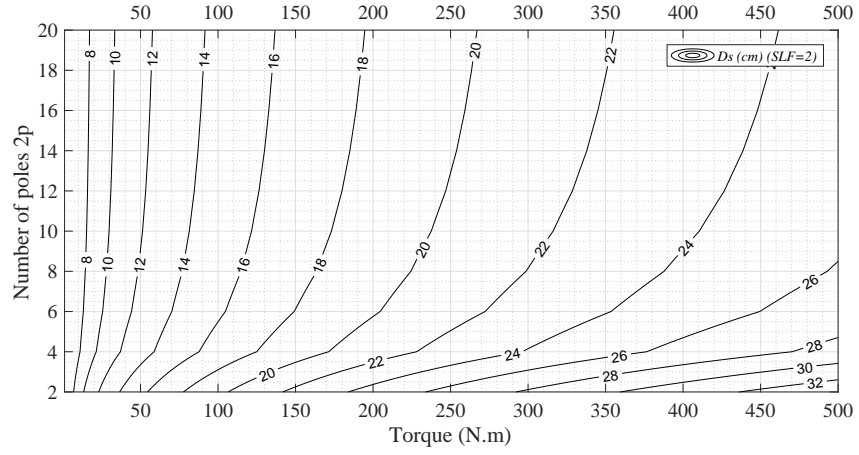


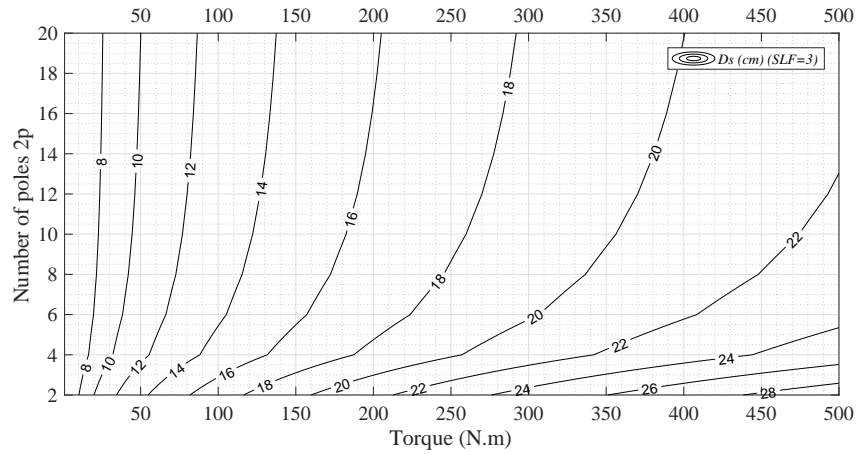
Fig. 14 L_t (cm) variations with torque T and SLF factor for $\sigma = 35 \text{ kPa}$.



(a) $D_s(T, p)$ for $SLF = 1$.



(b) $D_s(T, p)$ for $SLF = 2$.



(c) $D_s(T, p)$ for $SLF = 3$.

Fig. 15 D_s (cm) variations with torque T and number of poles p for $\sigma = 35kPa$.

Stator yoke thickness t_y is calculated using an analogy with the RFM formulae [14] where the RFM external rotor diameter is replaced by the average radius R_{av} of the AFM, such that:

$$t_y = \frac{B}{B_y} \times \frac{2 \cdot \pi \cdot R_{av}}{4 \cdot p} \quad (26)$$

where B/B_y is again the ratio between the magnetic loading B (average air-gap magnetic flux density) and the peak yoke flux density B_y , and p is the number of pole pairs. Slot depth l_s is a function of current linear intensity, current density, and various coefficients related to the materials and slot shape used[15]. For simplistic purposes, and based on experimental size comparisons, l_s is assumed to be approximately $1/3$ of R_o . The air gap width is assumed to be 2mm and the rotor thickness t_r is assumed to be equal to $0.1 \times 2 \cdot R_o$ for stress and integrity purposes [15]. Hence a simple mathematical model capable of predicting width L_t and outer diameter R_o of a typical AFM as a function of torque has been made.

As stated previously and unlike the RFM, the AFM configuration can be significantly boosted in terms of torque for a given diameter. This is achieved by adding another stator, and set of magnetic materials on the other side of the rotor, as shown in Fig.10b in slight transparency. Thus for approximately the double of L_t (and therefore volume), the rated torque T of the machine doubles. Indeed, the air-gap area A_{agap} effectively doubles which, following Eqn.23, leads to a doubling in rated torque capability. This is of particular interest in situations where the radial dimensions is strictly constrained. Note that the AFM width equation now becomes:

$$L_t = t_s + 2 \cdot (t_y + l_s + g + t_r) \quad (27)$$

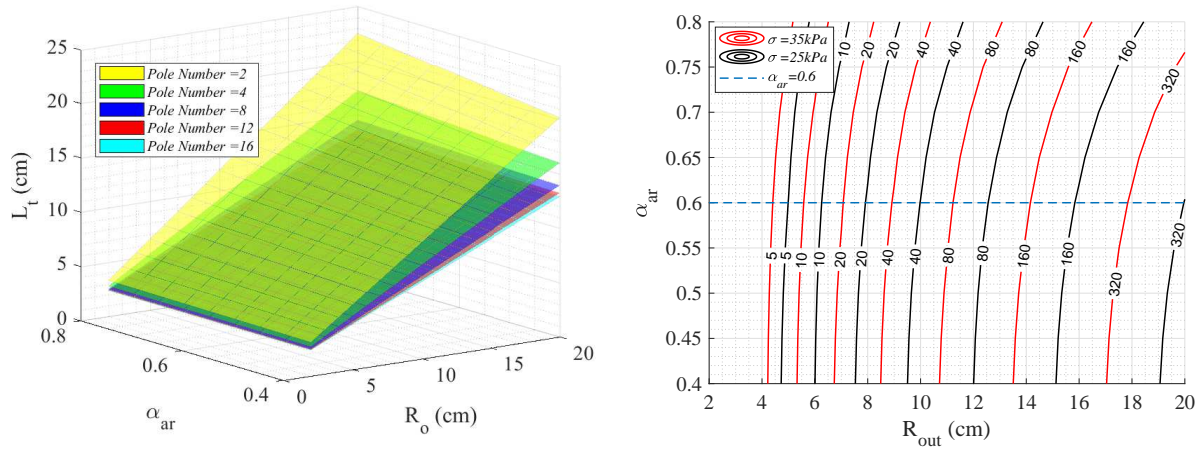
as rotor disc width is doubled to account for the torque doubling. Eqn.24 relating torque T as a function of R_o and α_{ar} must also be changed to:

$$T = 2 \times \sigma \times \pi \cdot R_o^3 \left(1 + \alpha_{ar} - \alpha_{ar}^2 - \alpha_{ar}^3 \right) \quad (28)$$

In both cases, the machine volume V_{afm} is given by:

$$V_{afm} = L_t \times \pi \cdot R_o^2 \quad (29)$$

It might also be of interest to the reader that such machines develop even more torque per volume (higher torque density) in non diameter restricted conditions. By increasing the R_o , greater torque increases are achieved for a given volume than by adding another stator [14]. In fact, it can be proven using the above equations that in the later case, a doubling of torque would require a new radius of $2^{1/3} \cdot R_o$, leading to a new volume of $2^{2/3} \cdot V_r$, instead of roughly double in the two stator configuration.



(a) Variations in $L_t(R_o, \alpha_{ar}, p)$, highlighting the impact of pole number on t_y

(b) Variations in $T(R_o, \alpha_{ar}, \sigma)$

Fig. 16 Variations in axial flux machine sizing variables following Eqn.20 to Eqn.26

Furthermore, it can be established by this mathematical model, and confirmed by experimental data [15], that the number of pole will greatly influence the width L_t of the machine, as the yoke thickness increases drastically as the number of pole $2.p$ drops. This is illustrated in Fig.16a which highlights the impact of AFM outer radius R_o , α_{ar} and the number of poles on L_t . Hence, to gain full benefits of the flatter AFM over the RFM, a sufficiently large number of poles must be used (over 8) which also increases machine cost (in material and complexity) and decreases rpm for a given power and signal frequency. Lastly, a contour of the torque for a single stator AFM is given against R_o and α_{ar} in Fig.16b. The effect of shear stress σ as well as torque expectations for a conventional $\alpha_{ar} = 0.6$ are highlighted in this graph.

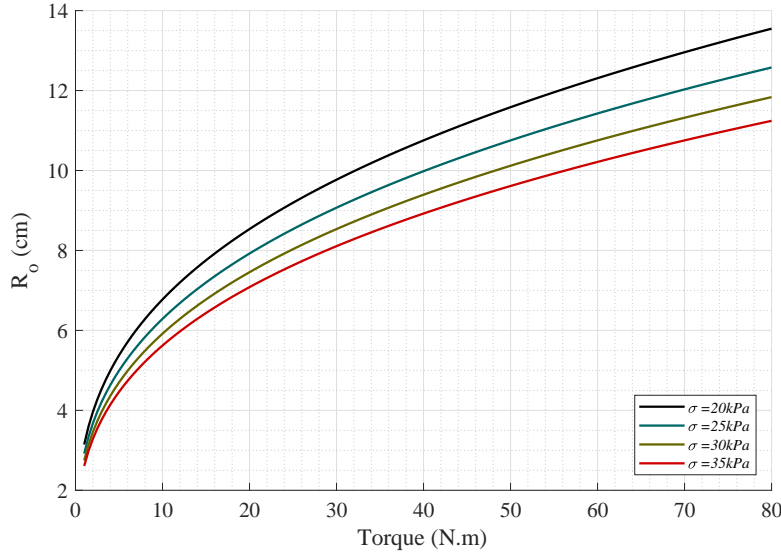


Fig. 17 R_o (cm) variations with torque T and shear stress σ

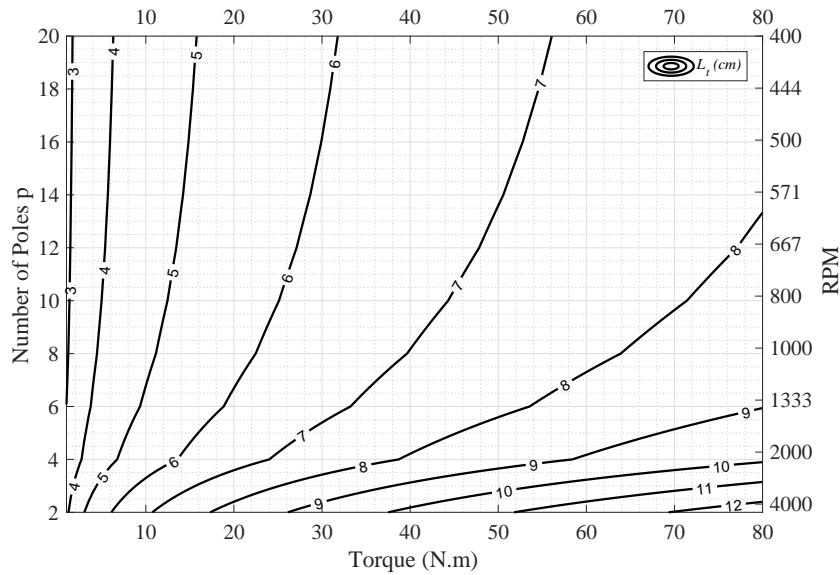


Fig. 18 L_t (cm) variations with torque T and pole number $2p$

A couple of useful charts have also been provided in Fig.17 and Fig.18. The first illustrates the variation in actuator radius as a function of desired torque and magnetic shear stress σ of the machine. Once again, it can be seen that machines of smaller dimensions are obtained by using higher σ values. The latter chart highlights the variations in machine total length L_t for a single stator machine, as a function of the number of poles (impact on t_y) and required

torque T . For a double stator machine, the reader is encouraged to either double L_t , which would give an appropriate estimate, or derive the new length from Eqn.27 and use the appropriate assumptions. These two charts can be used to quickly size an AFM machine when both torque requirements and sizing limitations of specific test cases are known.

D. Electric Motor Empirical Validation

Having established the theoretical models of both RFM and AFM elements, sizing results were compared against off-the-shelf motors from different manufacturers for validation. Due to the lack of data provided by some providers regarding their products, namely stack length, magnetic shear stress and even number of poles, some guess work had to be done in order to get realistic and coherent values in both parameters and size of the machine. Data from the motors used for validation and theoretical model results are given in Table 2 and Table 3 respectively for RFM and AFM motors which were found in various data sheets from different manufacturers [9, 11, 16, 17]. Known parameters from manufacturers data sheets are given in bold, whilst estimated values are in normal font. Various models from a number of manufacturers were used to cover a significant part of the torque spectrum and capture differences in manufacturing trends.

Bosch Rexroth	$T(N.m)$	$L_t(\Delta\%)(mm)$	$D_s(\Delta\%)(mm)$	$\sigma(kPa)$	SLF	$2p$	$m(kg)$
MS2N06-D1BNN	41,8	224	116	-	-	10	9
Model Results	41,8	199(-11%)	112(-3%)	35	2	10	-
	41,8	219(-2%)	104(-10%)	35	2,5	10	-
	41,8	240(7%)	135(16%)	20	2	10	-
Bosch Rexroth	$T(N.m)$	$L_t(\Delta\%)(mm)$	$D_s(\Delta\%)(mm)$	$\sigma(kPa)$	SLF	$2p$	$m(kg)$
MS2N06-B1BNN	10,2	164	90	-	-	10	5,1
Model Results	10,2	150(-9%)	84(-7%)	20	2	10	-
Kollmorgen	$T(N.m)$	$L_t(\Delta\%)(mm)$	$D_s(\Delta\%)(mm)$	$\sigma(kPa)$	SLF	$2p$	$m(kg)$
AKM63G	42,1	197	138	-	-	10	11,1
Model Results	42,1	217(10%)	149(8%)	20	1,5	10	-
	42,1	201(2%)	138(0%)	25	1,5	10	-
Kollmorgen	$T(N.m)$	$L_t(\Delta\%)(mm)$	$D_s(\Delta\%)(mm)$	$\sigma(kPa)$	SLF	$2p$	$m(kg)$
AKM42G	11,5	148	84	-	-	10	3,4
Model Results	11,5	131(-11%)	89(6%)	25	1,5	10	-
	11,5	141(-5%)	96(14%)	20	1,5	10	-
Ashwoods	$T(N.m)$	$L_t(\Delta\%)(mm)$	$D_s(\Delta\%)(mm)$	$\sigma(kPa)$	SLF	$2p$	$m(kg)$
IPM-200-33	45	207	106	-	-	-	10
Model Results	45	207(0%)	80(-24%)	20	0.6	10	-
	45	201(-3.5%)	71(-33%)	25	0.6	10	-
	45	192(-7%)	62(-41%)	30	0.6	10	-
Ashwoods	$T(N.m)$	$L_t(\Delta\%)(mm)$	$D_s(\Delta\%)(mm)$	$\sigma(kPa)$	SLF	$2p$	$m(kg)$
AKM42G	90	206	139	-	-	-	17
Model Results	90	211(3%)	123(-11.5%)	25	1	10	-
Other	$T(N.m)$	$L_t(\Delta\%)(mm)$	$D_s(\Delta\%)(mm)$	$\sigma(kPa)$	SLF	$2p$	$m(kg)$
	159	214	258	-	-	-	24,2
Model Results	159	224(5%)	277(7%)	35	0,5	10	-
	159	224(5%)	284(10%)	35	0,5	8	-

Table 2 RFM off-the-bench comparison with model prediction results.

It is clear from these results that, unlike the hydraulic piston sizing, the confidence in actuator sizing is significantly lower. Divergence from prediction to product data differs in varying amount throughout the torque spectrum, ranging up to 15% in diameter and/or length. Despite of this, realistic parameters were nearly always found so as to predict

GKN	$T(N.m)$	$L_t(\Delta\%)(mm)$	$D_s(\Delta\%)(mm)$	$\sigma(kPa)$	$n^\circ stator$	$2p$	$m(kg)$
EVO AF130	170	110	300	-	1	-	30.5
Model Results	170	102.8(-6.5%)	289(-3.5%)	35	1	10	-
GKN	$T(N.m)$	$L_t(\Delta\%)(mm)$	$D_s(\Delta\%)(mm)$	$\sigma(kPa)$	$n^\circ stator$	$2p$	$m(kg)$
EVO AF140	260	115.2	380	-	1	-	42.5
Model Results	260	116.6(1%)	334(-12.1%)	35	1	10	-
GKN	$T(N.m)$	$L_t(\Delta\%)(mm)$	$D_s(\Delta\%)(mm)$	$\sigma(kPa)$	$n^\circ stator$	$2p$	$m(kg)$
EVO AF230	340	212	300	-	2	-	57.5
Model Results	340	196(-7.5%)	289(-3.5%)	35	2	10	-
GKN	$T(N.m)$	$L_t(\Delta\%)(mm)$	$D_s(\Delta\%)(mm)$	$\sigma(kPa)$	$n^\circ stator$	$2p$	$m(kg)$
EVO AF240	520	224	380	-	2	-	82
Model Results	520	223(-0.5%)	334(-12.1%)	35	2	10	-
Ashwoods	$T(N.m)$	$L_t(\Delta\%)(mm)$	$D_s(\Delta\%)(mm)$	$\sigma(kPa)$	$n^\circ stator$	$2p$	$m(kg)$
IPM-200-33	45	80	260	-	1	-	13
Model Results	45	82(2.5%)	230(-11.6%)	20	1	10	-

Table 3 AFM off-the-bench comparison with model prediction results.

the size of the motor within acceptable error margins. Errors can easily be explained by the lack of confidence in the estimations for stack length factor, magnetic shear stress and number of poles used during the comparison, but also on manufacturing preferences. Each designer will tend to manufacture and assemble products differently, which the sizing tool does not account for. This directly leads to errors in length L_t as the prediction model only sizes the absolute physical requirements with an empirical sizing factor, for indicative purposes (use of the l_f factor in Eqn. 19). The value for $l_f = 0.75$ was found acceptable for conventional RFM. But it can be seen that comparison in length with the Ashwood designs in Table 2, described as dense and lightweight, falls quite short. This is because the length used here is that of the stator stack length only, as the real geometry of the motor does not include much additional axis length. Hence $l_f = 0.75$ leads to even worse results. This is an obvious limitation of the simplistic length correction. Furthermore, some of these device may incorporate cooling systems (water or air) or brakes (when brakes were clearly stated, brake length were subtracted from total) which will impact both dimensions of the motor. It does also arguably impact the weight of the motors significantly more.

Nonetheless, the capability of estimating the size of an electric motor, be it of AFM or RFM type for a given torque requirement, or vice versa, with a 15% margin was achieved, an acceptable accuracy for the rapid sizing tool set. By applying a safety margin, space allocation can be made for further design, knowing that sufficient care has been taken to ensure an appropriate actuator can be included in the system. Comparison against off-the shelf motors not only provided validation but also weights of some typical designs. Therefore, with more data points, a weight estimation against torque or volume can be made to predict actuator mass.

IV. System Sizing Example

A couple of test case examples will be used to illustrate the potential of the tools presented herein. Firstly, a landing gear deployment system will be sized making the assumption that a hydraulic piston is used as an actuator. Then, an electric motor will be sized for a wing mounted control surface with an electric rotor actuator combined with appropriate gearbox solutions.

A. Landing gear deployment system

From loads calculation, an estimation of the moment to deploy the main landing gear of an illustrative aircraft was provided. Assuming a piston actuator, attachment points on the landing gear have also been determined, leading to a given lever arm length and therefore force requirement. Stroke length required to extend the gear completely can be assumed using a geometrical analysis, or simply be given as well. It is also assumed that the system hydraulic pressure is $5kPsi$ and that the piston must be able to operate with 20 bar of pressure in the non pressurised chamber, with a 1.5

safety factor on piston structural integrity. With this set of parameters, the LHyAS tool for piston sizing can be used, to determine the diameter and length of the actuator, rod diameter and wall thickness. A crude yet accurate sketch of the landing gear system is given in Fig.19. System and LHyAS results are summarised in Table 4.

With desired stroke and actuator force as inputs, the tool gives estimates of length and diameter values directly. Using contour charts similar to Fig.7 and Fig.8 charts, it is also easy to grasp the impact of changing both force and stroke length requirements, a possible useful input to combine with landing gear design if space becomes problematic: a possible change in lever arm or piston rotational joint could potentially reduce actuator size whilst remaining within acceptable structural loads.

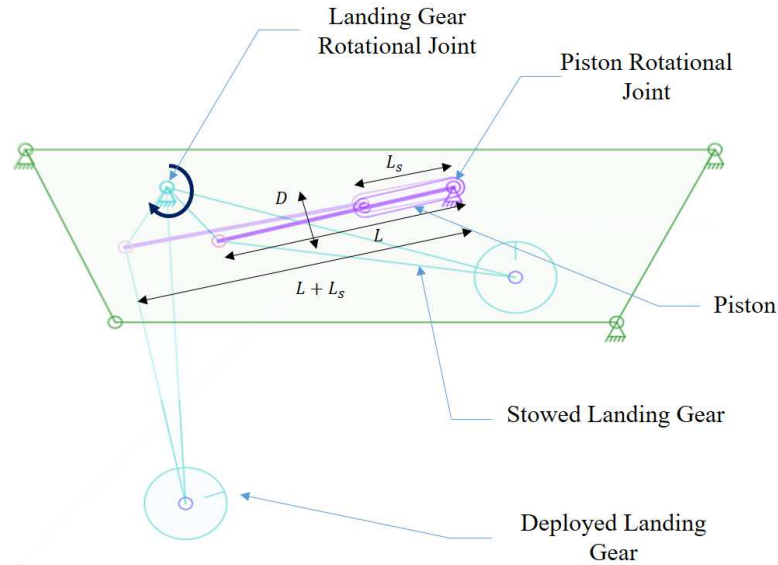


Fig. 19 Piston schematics for unbalanced and balanced actuators

Force Required	$F(kN)$	400
Stroke Required	$L_s(mm)$	500
Operating Pressure	$P_1(bar)$	345
Residual Pressure	$P_2(bar)$	20
Safety Factor	S_f	1.5
Length	$L(mm)$	1194
Outer Diameter	$D(mm)$	180
Rod Diameter	$D_r(mm)$	31.2
Wall Thickness	$t_y(mm)$	12.8

Table 4 Landing gear sizing parameters

Torque Required	$T(N.m)$	20
Magnetic Shear Stress	$\sigma(kPa)$	35
Number of poles	$2p$	10
RFM (SLF=1)		
Outer Diameter	$D_s(mm)$	110
Length	$L_t(mm)$	125
AFM (1 stator)		
Outer Diameter	$D_o(mm)$	141
Length	$L_t(mm)$	57

Table 5 Electric motor sizing parameter comparison example

B. Control surface actuation

Having sized the control surfaces for adequate aircraft response, an estimate of the aerodynamic loading of the control surface, and therefore on the rotation hinge can be derived. Assuming such data was provided, along with estimates of the desired rotation speed of the controls, a trade-off between the gear box reduction ratio, hinge moment, and machine torque can be found. Let us assume that the target machine will have a nominal rpm of 2000, and a reduction ratio of 300 (achievable through multi-stage epicyclic reduction complemented with optional rotary screw transmission for instance) can be used. This allows for the control surface under an hypothetical maximum hinge moment of $5kN.m$ to be driven by a machine with a maximum torque $16.7N.m$, rounded at $20N.m$ to account for

non unit efficiency of each component along the power transmission chain. Using the RFM and AFM sizing tools, appropriate motor sizes can be derived. Motor assumptions and sizing results are given in Table 5 for both AFM and RFM machines. Given available wingbox size, advised decisions can be made regarding the best technology to use, and potential changes to the reduction chain. Given the size of the machine, a volume and mass estimate can also be made further complementing the prototype design.

V. Conclusions and Further Work

A. Conclusion

The sizing tools developed and presented herein were developed as part of a systems sizing project led by Cranfield University and supported by Airbus Group. These tools are aimed at providing rapid and accurate sizing estimates of various actuators using physics based models for a variety of aerospace applications. The physics based assumptions allows engineers to estimate specialised manufacturer capability, or plausible off-the shelf product capability given specific design requirements. Both linear hydraulic and rotary electric conventional actuators were considered.

Based on simple mathematical formulations and assumptions, simple physics based formulation have been derived, suitable for a variety of software environments. Compared to other actuator sizing tools found in the literature, this physics based formulation allows for more accurate control over specific parameters, unlike the scaling or database interpolation methods. Using a relatively small set of geometric variables and design parameters, an estimate of actuator size, and therefore weight and volume based on force or torque requirements can be obtained. The tools were constructed to be used reversibly as well. Engineers with basic system knowledge and generic software such as Matlab or Excel can find the required details to reproduce and use the models presented herein.

Validation of the method was carried out against commercial and off-the-shelf actuators. The linear hydraulic actuator model showed a $\pm 2\%$ deviation compared to an Airbus in-house database in both length and diameter for forces between $30kN$ to $600kN$, exceeding the authors initial expectations of the tool. The AFM and RFM electric motor sizing tools have led to results varying by up to $\pm 15\%$ in length or diameter when compared to commercial off-the-shelf products. This lower accuracy was linked to the wider range of uncertainty on parameters and complexity of the latter tools. Nonetheless, these results were accepted as satisfactory for early prototyping and design stages of actuation systems, prior to more complete specific design studies.

A set of very simple use cases have also been included to demonstrate the methodology and results of the tools presented herein. Given the wide range of force and torque considered, the authors believe that this approach to actuator sizing could be used not only for sizing actuators suitable for large aircraft applications, but large wind-tunnel models, reduced scale advanced flight demonstrators and large UAVs. Care should be taken when scaling to smaller RC models to account for the growing impact of non-physics related system component size (structure, attachments, wires, etc.).

Note that with the recent interest in SMA for in-flight actuation due to their high power densities [4, 5, 18], anyone investigating system actuation should consider this approach to conventional actuator sizing for a rapid comparison. Thus will the user appreciate the limits of the conventional actuators given a set of spatial limitations, and understand the achievable torque or force densities. These can then be compared against newer solutions, which may, or may not, be suitable for the considered applications. After all, SMA's do have larger torque densities when used as SMA rods for instance, but lack actuation speed, require accurate thermal control capability and still have more complex development, implementation processes and life cycle management [2, 3, 19].

B. Further Work

Just like any tool, these sizing models can be further improved, both in terms of result accuracy and user experience. A key function that can be easily added is a direct link from size, and therefore volume, and mass of the actuators. This can be validated against off-the-bench data but can still be made using physics based modelling assumptions as a function of materials used and overall actuator density. Initial estimate methods developed by the authors and not included herein have proven to be as accurate as sizing results ($\pm 10\%$), and rely on material density and system empty-to-full ratio estimates obtained from the various geometric parameters. Regarding model accuracy, additional off-the-bench comparisons throughout the force and torque spectrum can be made to increase result confidence. Sizing corrections could also be further fine tuned for the electric motors, especially in terms of length, for the different manufacturers.

To further complement this set of actuators, one could consider a gear box sizing framework used in conjunction with the electric motor sizing tool. A power-hinge sizing tool not included herein was concurrently developed by the

authors to predict gearbox size as a function of reduction ratio and torque requirements. Parameters such as number and gear diameter, tooth size and number, arrangements can be used to size gear boxes meeting specific gear ratios requirements through simple gear theory equations. Similarly, linear roller screw systems are considered in further work.

Lastly, user experience could be further improved by creating graphical user interfaces when setting up the sizing tool, and exporting results in CAD acceptable format for automatic object generation. This would allow for a seamless shift from torque requirements to sized cylinders or rectangular box mimicking electric motors or pistons to be included within the design space of interest, *ie.* wing box, fuselage, etc.

Acknowledgments

This work is supported and developed by Cranfield University and in collaboration with Airbus Group and Innovate UK as part of the Aircraft Wing Integration research project.

References

- [1] Chakraborty, I., Trawick, D. R., Jackson, D., and Mavris, D., “Electric Control Surface Actuator Design Optimization and Allocation for the More Electric Aircraft,” *2013 Aviation Technology, Integration, and Operations Conference*, American Institute of Aeronautics and Astronautics, Reston, Virginia, 2013. doi:10.2514/6.2013-4283.
- [2] Hartl, D. J., and Lagoudas, D. C., “Aerospace applications of shape memory alloys,” *Proceedings of the Institution of Mechanical Engineers, Part G: Journal of Aerospace Engineering*, Vol. 221, No. 4, 2007, pp. 535–552. doi:10.1243/09544100JAERO211.
- [3] Thill, C., Etches, J., Bond, I., Potter, K., and Weaver, P., “Morphing skins,” *Aeronautical Journal*, Vol. 112, No. 1129, 2008, pp. 117–139.
- [4] Weber, A., “Shape-Memory Alloys Help NASA Create New Wing Design | 2018-03-05 | Assembly Magazine,” , 2018. URL <https://www.assemblymag.com/articles/94169-shape-memory-alloys-help-nasa-create-new-wing-design>.
- [5] Kamlet, M., “NASA Tests New Alloy to Fold Wings in Flight,” , 2018. URL <https://www.nasa.gov/centers/armstrong/feature/nasa-tests-new-alloy-to-fold-wings-in-flight.html>.
- [6] Munjulury, R. C., Andrés, I. E., Diaz Puebla, A., and Krus, P., “Knowledge-based Flight Control System and Control Surfaces Integration in RAPID,” *Aerospace Technology Congress*, Stockholm, 2016.
- [7] Budinger, M., Liscouet, J., Lefevre, Y., Fontchastagner, J., Abdelli, A.-N., and Allain, L., “Preliminary design of electromechanical actuators with Modelica,” *7th Modelica Conference*, 2009. doi:10.3384/ecp09430099.
- [8] Budinger, M., Reyssset, A., Halabi, T. E., Vasiliu, C., and Maré, J.-C., “Optimal preliminary design of electromechanical actuators,” *Proceedings of the Institution of Mechanical Engineers, Part G: Journal of Aerospace Engineering*, Vol. 228, No. 9, 2014, pp. 1598–1616. doi:10.1177/0954410013497171.
- [9] GKN, “GKN Electric Vehicle Technology. Technical Datasheet,” Official Website, <https://www.gknlandsystems.com>, 2013.
- [10] Magnax, “Magnax Axial Flux Direct Drive Machine,” Official Website, <https://www.magnax.com/product>, 2018.
- [11] Ashwoods, “Ashwoods Electric Motors | AEM,” Official Website, <https://ashwoodselectricmotors.com/>, 2018.
- [12] Miller, T. J. E., *Brushless Permanent-Magnet and Reluctance Motor Drives*, Oxford University Press, Oxford, New York, 1989.
- [13] Soong, W., “Sizing of electrical machines,” Tech. Rep. 2, Power Engineering Briefing Notes, 2008. URL <http://www.eleceng.adelaide.edu.au/research/power/pebn/pebn009sizingofelectricalmachines.pdf>.
- [14] Patterson, D. J., Colton, J. L., Mularcik, B., Kennedy, B. J., Camilleri, S., and Rohoza, R., “A comparison of radial and axial flux structures in electrical machines,” *2009 IEEE International Electric Machines and Drives Conference, IEMDC '09*, 2009, pp. 1029–1035. doi:10.1109/IEMDC.2009.5075331.
- [15] Parviainen, A., “Design of Axial-Flux Permanent-Magnet Low-Speed Machines and Performance Comparison Between Radial-Flux and Axial-Flux Machines,” Phd, Lappeenranta University of Technology Asko, 2005.
- [16] Kollmorgen, “Motion Control Solutions | Kollmorgen | Industrial Servomotors Servo Drives AC DC Motors,” Official Website, <https://www.kollmorgen.com/en-us/>, 2018.

- [17] Bosch-Rexroth, "Bosch Rexroth. The Drive & Control Company. - Bosch Rexroth Great Britain," Official Website, <https://www.boschrexroth.com/en/gb/>, 2018.
- [18] Sofla, A., Meguid, S., Tan, K., and Yeo, W., "Shape morphing of aircraft wing: Status and challenges," *Materials and Design*, Vol. 31, 2009, pp. 1284–1292.
- [19] Noebe, R. D., Susan, L. D., Nathal, M. V., and Garg, A. G., "High work output NI-TI-PT high temperature shape memory alloys and associated processing methods," , 2006.

2019-01-06

Size estimation tools for conventional actuator system prototyping in aerospace

Dussart, Gaétan

American Institute for Aeronautics and Astronautics

Dussart GX, Lone MM and O'Rourke C., Size estimation tools for conventional actuator system prototyping in aerospace. AIAA Scitech 2019 Forum, San Diego, 7-11 January 2019.

<https://dspace.lib.cranfield.ac.uk/handle/1826/13890>

Downloaded from Cranfield Library Services E-Repository